

Alma Mater Studiorum Università di Bologna  
Archivio istituzionale della ricerca

Evolution of drop size distribution in natural rain

This is the final peer-reviewed author's accepted manuscript (postprint) of the following publication:

*Published Version:*

D'Adderio, L.P., Porcù, F., Tokay, A. (2018). Evolution of drop size distribution in natural rain. *ATMOSPHERIC RESEARCH*, 200, 70-76 [10.1016/j.atmosres.2017.10.003].

*Availability:*

This version is available at: <https://hdl.handle.net/11585/621190> since: 2018-02-12

*Published:*

DOI: <http://doi.org/10.1016/j.atmosres.2017.10.003>

*Terms of use:*

Some rights reserved. The terms and conditions for the reuse of this version of the manuscript are specified in the publishing policy. For all terms of use and more information see the publisher's website.

This item was downloaded from IRIS Università di Bologna (<https://cris.unibo.it/>).  
When citing, please refer to the published version.

(Article begins on next page)

This is the final peer-reviewed accepted manuscript of:

Leo Pio D'Adderio, Federico Porcù, Ali Tokay, Evolution of drop size distribution in natural rain, Atmospheric Research, Volume 200, 2018, Pages 70-76.

The final published version is available at:  
<https://doi.org/10.1016/j.atmosres.2017.10.003>

#### Rights / License:

The terms and conditions for the reuse of this version of the manuscript are specified in the publishing policy. For all terms of use and more information see the publisher's website.

*This item was downloaded from IRIS Università di Bologna (<https://cris.unibo.it/>)*

***When citing, please refer to the published version.***

1                                   **Evolution of Drop Size Distribution in natural rain**

2  
3  
4  
5                                   Leo Pio D’Adderio

6                                   Dep. of Physics and Earth Science, University of Ferrara, Italy,

7  
8                                   Federico Porcù

9                                   Dep. of Physics and Astronomy, University of Bologna, Italy

10  
11                                  Ali Tokay

12   JCET-University of Maryland Baltimore County and NASA-Goddard Space Flight Center, Greenbelt,  
13                                  Maryland, USA.

14  
15  
16  
17  
18  
19   Corresponding author: Leo Pio D’Adderio, Department of Physics and earth Science, University of Ferrara,  
20   44122, Ferrara, Italy  
21   Email: dadderio@fe.infn.it  
22

## Abstract

Both numerical modeling and laboratory experiments document the possibility of a raindrop size distribution (DSD) to evolve to an equilibrium stage (EDSD), where all the principal processes occur at steady rates.

The aim of this work is to observe the temporal behavior of the DSD and to directly investigate the conditions favorable to the onset of the EDSD in natural rain. We exploited a large disdrometer dataset collected in the framework of the Ground Validation activities related to the NASA Global Precipitation Measurement mission. More than 200,000 one-minute data of two-dimensional video disdrometer (2DVD) are collected over USA to represent a wide range of precipitation types. The original data are averaged over 2 minutes and an automatic algorithm is used on a selected subset to identify samples with EDSD. Results show that the EDSD occurs mainly in convective events and lasts for very short time intervals (2 to 4 minutes). It is more frequent for rain rate between 20 and 40 mm h<sup>-1</sup> and it mostly occurs during sharp increase of precipitation rates.

45	Keywords
46	Equilibrium Drop Size Distribution
47	Time evolution
48	Collisional breakup
49	Breakup detection algorithm
50	Radarmeteorology
51	

## 1. Introduction

The Drop Size Distribution (DSD) is a fundamental property of precipitation and is widely investigated through laboratory, numerical modeling and field studies. A detailed knowledge of DSD structure and variability is required in remote sensor based precipitation retrieval algorithms (Tokay et al., 2016), in cloud resolving models (Tao et al. 2014) and in application to soil science and agriculture (Caracciolo et al, 2012).

From the cloud microphysics point of view, the DSD shape at the ground is determined in natural rain by the complex interplay of a number of mechanisms (Radhakrishna and Rao, 2009), where the collisional breakup is known as the process that limits the maximum raindrop size (McTaggart-Cowan and List, 1975; Barros et al., 2010). A large raindrop falling within or below a cloud and colliding with smaller drops, forms a larger raindrop when the Collisional Kinetic Energy (CKE) is lower than a limiting value (about 5  $\mu\text{J}$ ), while larger CKE values indicate that the energy cannot be dissipated by the viscous motions of the merged drop, and the drop breaks up (Low and List, 1982a, Porcù et al., 2013). The drop disruption leads to a number of fragments with a well-defined distribution: one peak at size slightly smaller than the largest colliding drop, and one peak at very small drop size (Low and List, 1982a). Schlottke et al. (2010), who simulated the Low and List (1982a) experiment, found that collisional breakup takes place even for CKE slightly lower than 5  $\mu\text{J}$ , in cases of grazing collisions.

The combined effect of coalescence and collisional breakup has been studied mainly by simulations in numerical models, focusing on the shape variation of the initial DSD up to reach the so-called equilibrium stage, described by the Equilibrium DSD (EDSD). The parameterization proposed by Low and List (1982a,b) of breakup fragments is taken as reference in most of the numerical schemes to simulate DSD evolution in time until the EDSD is reached. While early studies concerning this topic

found a three-peak EDSD (Valdez and Young, 1985; Brown, 1988; Feingold et al., 1988; Chen and Lamb, 1994), McFarquhar (2004) derived a different parameterization of the breakup fragments, leading to a different shape of the EDSD with respect to the previous works. Starting from an initial exponential DSD corresponding to  $54 \text{ mm h}^{-1}$  rainfall rate, the resulting EDSD presents a bi-modal shape with the peaks at 0.26 and 2.3 mm. Prat and Barros (2007), using a discrete model, found that the EDSD has the same shape (bi-modal) independently from the initial DSD and for the same rainfall rate and breakup kernel, with marked difference in the time required to reach the EDSD. In their follow-up studies, deepening the influence of the microphysical processes on Z-R relationship (Prat and Barros, 2009), they found that, in general, for rain rates lower than  $20 \text{ mmh}^{-1}$  the coalescence is the dominant process. For higher rain rates, the breakup is the dominant process and the time to reach the EDSD is about half as long as in the case of light rainfall (about 30 minutes compared with at least one hour). Moreover, they found that for heavy rain the sensitivity of the DSD shape to the rain rate is negligible. More recently, Prat and Barros, (2012) developed a new parameterization of the fragments of the drop-drop collision leading to EDSD with a lower number of large drops. This evidences that the EDSD can be reached at lower rainfall rate regimes than what they previously found.

As also highlighted by McFarquhar (2004), the literature is scant of EDSD observations from natural rain. While the numerical model outputs allow for monitoring rain DSDs resulting from coalescence and breakup events at every time stamp, thus unambiguously assessing the EDSD onset, the detection of EDSD in natural rain is more questionable. Hu and Srivastava (1995) tried to compare their model output with disdrometer observations noticing that in addition to the bi-modal shape, a slope in the large drops tail of observed DSD around  $20 \text{ cm}^{-1}$  can be taken as a signature of EDSD, shaped by collisional processes. However, this result could be affected by the known problem of Joss Waldvogel disdrometer in detecting large drops.

100 A further characteristic of the EDSD is the bi-modality. Porcù et al. (2013, 2014) observed bi-modal  
101 DSD shape from measurements at different altitudes using a low power X-band Doppler  
102 disdrometer. The position of the DSD peaks agrees quite well with that obtained by different  
103 numerical models, even though there was altitude dependence. Bi-modal DSDs were also observed  
104 by Steiner and Waldvogel (1987), Zawadzki and de Agostinho Antonio (1988), List et al. (1988), and  
105 Asselin de Beauville et al. (1988), which all used Joss-Waldvogel disdrometer. Willis and Tattelman  
106 (1989) also observed bi-modal DSD at very high rainfall rates collected during hurricanes and tropical  
107 storms using an optical spectrometer. However, bi-modality does not seem to be a sufficient  
108 condition to have EDSD, since other cloud processes are able to produce bi-modal DSD  
109 (Radhakrishna and Rao, 2009). Based on both theoretical studies and experimental observations,  
110 D’Adderio et al. (2015) developed an automatic algorithm to identify bi-modal DSD (with peaks in  
111 well defined diameter ranges) and labeled them as EDSD, analyzing two-minutes samples from six  
112 different field campaigns. They found that, in natural rain, the reaching of the EDSD is rare (at most  
113 7% of the analyzed samples) and occurs mainly during convective precipitation.

114 In this paper, by using the D’Adderio et al. (2015) algorithm, the conditions favorable to reach the  
115 EDSD in natural rain have been studied. To this end, an extensive disdrometer dataset, collected  
116 during several field campaigns in the framework of the NASA/JAXA Global Precipitation  
117 Measurement Mission (GPM) ground validation (GV) activities, is analyzed to extract EDSD samples  
118 in natural rain. The automatic algorithm developed by D’Adderio et al. (2015), based on the slope  
119 of the DSD curve between 1.0 and 2.6 mm, is used to select the EDSD samples as collected by the  
120 two-Dimensional Video Disdrometer (2-DVD).

121 We remark that the GPM GV field campaigns, although providing a large amount of high quality  
122 disdrometric data, were not planned to study DSD properties at cloud scale. A dedicated field  
123 campaign would be desirable to complete the results of the present work allowing a lagrangian



observation of the cloud to assess the full temporal evolution of the EDS in the same developing cloud column.

The paper is organized as follow: Section 2 presents a brief description of the field campaigns characteristics useful to our aim; a critical description of the algorithm to identify the EDS is given in Section 3, while Section 4 and Section 5 describe the overall results obtained and some case study, respectively. The last section provides the conclusions.

## 2. Field Campaigns characteristics

This study uses the 2DVD (Schönhuber et al. 2007) observations from five different field campaigns of the GPM-GV program: Iowa Flood Studies (IFloodS – 41.6N, 91.5W from May 1 to June 15, 2013), Midlatitude Continental Convective Clouds Experiment (MC3E – 36.7N, 97.1W from April 22 to June 6, 2011), Wallops Flight Facility (Wallops – 37.5N, 75.5W from July 22, 2013 to October 7, 2015 not continuously), Integrated Precipitation and Hydrology Experiment (IPHEX – 35.5N, 82.5W from May 1 to June 15, 2014) and Alabama-Huntsville (Alabama – 35N, 87W from December 17, 2009 to October 13, 2011). The drop-by-drop raw output of the 2DVD was binned in 0.2 mm bin width and averaged over two minutes, called samples hereafter. Table 1 summarizes the characteristics of 2DVD observations relevant for our analysis in each field campaigns. The rightmost column reports the samples with positive Highest Slope (HS), which is the maximum slope of the linear fit of the DSD between 1.0 and 2.6 mm, defined in D’Adderio et al. (2015) that will be discussed in the next Section.

Field Campaign	Events	Samples	Stratiform Samples	Convective Samples	HS>0 Samples
Alabama	4	68		68	7
IFloodS	28	1016	63	953	48
IPHEX	14	368		368	28
MC3E	10	174		174	13
Wallops	75	1466	31	1435	133

Table 1. Characteristics of the dataset.

The number of rainfall events considered in the present work ranges from 4 for the Alabama dataset to 75 for the Wallops site (Table 1). An event is defined as set of at least 8 samples with rain rate exceeding  $1 \text{ mm h}^{-1}$  and reporting at least one EDSD selected according to the D'Adderio et al. (2015) algorithm. This has been considered a good compromise between having a sufficient time interval to follow the evolution of the precipitation, and to include stratiform precipitation that could lead to EDSD. Each event is identified as convective or stratiform according to Bringi et al. (2003): the classification is based on the standard deviation of the rain rates. If the standard deviation of the rain rates is  $\geq 1.5 \text{ mmh}^{-1}$ , then the event is considered convective otherwise it is considered stratiform. Ioannidou et al. (2016) used the same criterion to validate the measurements of the Precipitation Radar (PR) of the Tropical Rainfall Measuring Mission (TRMM) by comparing the rainfall estimates with 2DVD and X-band ground based radar measurements. Several authors conducted studies about the development of technique to characterize convective and stratiform precipitation. Among the others, Caracciolo et al. (2006) based their analysis using high order DSD moments, while Thurai et al. (2016) developed a separation technique in the  $N_w$ - $D_0$  space. Table 1 also shows that almost all the selected samples are classified as convective, while the last column reports the number of samples with EDSD occurrence.

Table 2 reports, for each dataset, the number of all registered convective and stratiform episodes, considered just as set of at least 8 samples with rain rate exceeding  $1 \text{ mm h}^{-1}$  regardless if EDSD is present or not. The percentage of episodes with EDSD (previously defined as event) ranges between

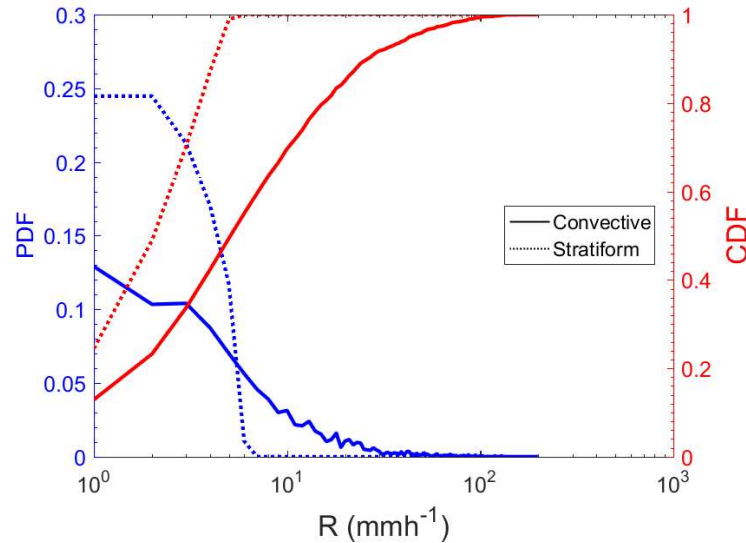
168 17 and 27% of cases selected according to our classification. All the datasets report a significant  
 169 number of stratiform episodes, even if only three present at least one EDSD sample. This aspect  
 170 highlights the strict relationship between the onset of EDSD and the convective precipitation.

Field Campaign	All Convective	Convective with EDSD	All Stratiform	Stratiform with EDSD
Alabama	15	4	12	0
IFloodS	143	26	123	2
IPHEX	80	14	33	0
MC3E	54	10	54	0
Wallops	154	74	212	1

171 Table 2. Convective/stratiform classification for the registered episodes.

172

173 Figure 1 shows the Probability Density Function (PDF – blue lines) and Cumulative Density Function  
 174 (CDF – red lines) of rain rate for the considered events (3,092 samples) after the  
 175 convective/stratiform discrimination (solid/dashed lines).



176 Figure 1. PDF (blue lines) and CDF (red lines) for convective (solid lines) and stratiform (dashed lines)  
 177 samples.

178 The rain rate of the stratified events presents a narrow distribution and never exceeds  $7 \text{ mm h}^{-1}$   
 179 with a marked peak around  $2 \text{ mm h}^{-1}$ . The PDF of the convective events is toward higher values, up  
 180 to more than  $100 \text{ mmh}^{-1}$ , and about the 30% of the samples has rain rate exceeding  $10 \text{ mm h}^{-1}$ .

181

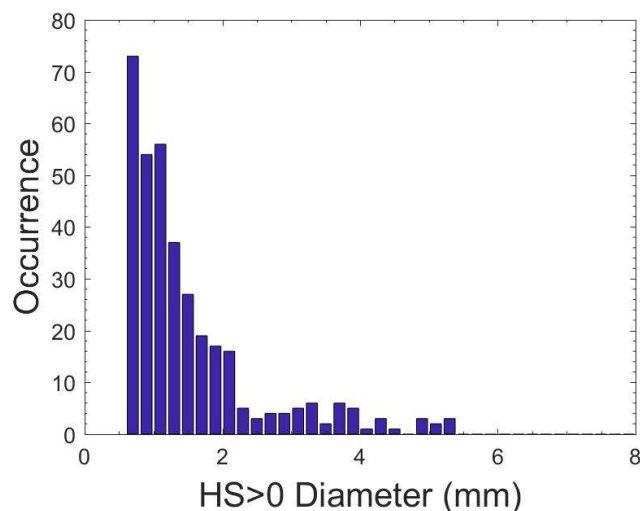
### 182 3. Equilibrium Drop Size Distribution detection algorithm

183 Following laboratory experiment results (Low and List, 1982a, b) and numerical modeling output  
184 (Prat and Barros, 2012), the EDSD bi-modal shape is characterized by: 1) a peak at very small drops  
185 end (around 0.3 mm) due to the breakup fragments; 2) a depletion in the region between 1.0 and  
186 1.5 mm due to the drops involved in the collisions; 3) a relative secondary maximum around 2.0  
187 mm. This is well observed in numerical simulations, where the EDSD shape is reached after a given  
188 time following the start of precipitation, and lasts indefinitely until a modification in the boundary  
189 conditions occurs (Prat and Barros, 2009).

190 An automated algorithm based on the slope (HS) of the linear fit of the DSD between 1.0 and 2.6  
191 mm has been introduced to identify and select the EDSD in natural rain (D'Adderio et al, 2015). The  
192 EDSD is present if the sample satisfies the condition  $HS > 0$ , i.e. the DSD shape shows the same  
193 features found in EDSD obtained by numerical modeling and laboratory experiments. This algorithm  
194 is applied to the samples with rain rate exceeding  $5 \text{ mmh}^{-1}$ , and the events where at least one  
195 sample has  $HS > 0$  have been selected for further processing.

196 As a matter of fact, the algorithm selects the DSD with positive slope between 1 and 2.6 mm in the  
197 diameter spectrum, which have been labeled as EDSD (D'Adderio et al, 2015). We are aware that  
198 other mechanisms can induce bi-modality in DSD: size sorting (related to updraft and vertical wind  
199 shear or to the beginning of the precipitation), coexistence of melted snowflakes and supercooled  
200 droplets, rainshafts overlapping, and any combination of these (Radhakrishna and Rao, 2009). It is  
201 difficult, if not impossible, to assess the contribution of each mechanism by analyzing the DSD shape  
202 in natural rain. We based the reliability of the results of the algorithm in identifying the EDSD on the  
203 correspondence with numerical studies and the discussion below.

204 In order to quantify the possible influence of the above-mentioned mechanisms in the EDSD  
 205 selection, the detection algorithm has been applied to a wider diameter spectrum, between 0.6 and  
 206 5.0 mm, seeking for  $HS > 0$ . We found 352 DSD samples, distributed with the size of the point  
 207 corresponding to  $HS > 0$  as shown in Figure 2. For most of the selected DSD (180; 51%) this point is in  
 208 the interval 1.0-2.6 mm, a large fraction (127; 36%) is between 0.6-1.0 and the reminders (45; 13%)  
 209 are distributed above 2.6 mm. Most of the DSD with positive HS in the interval 0.6-1.0 mm are not  
 210 bi-modal but can be due to the underestimation of small drops by 2DVD (Tokay et al. 2013) resulting  
 211 in a peak between 0.5 and 1.0 mm. The rest of the graph shows that positive HS can be found along  
 212 the diameter spectrum for all values, but its occurrence is much more frequent in the 1.0-2.6  
 213 interval. This analysis, in our view, supports our hypothesis of labeling as EDSD the DSD with positive  
 214 HS in this interval, since the other mentioned mechanisms producing bi-modal DSD are expected to  
 215 be distributed randomly without any preferential size. Even if we are confident that the DSD with  
 216 positive HS in the interval 1.0-2.6 mm are EDSD, we cannot exclude a marginal contamination from  
 217 DSD for which bi-modality is not due to equilibrium.

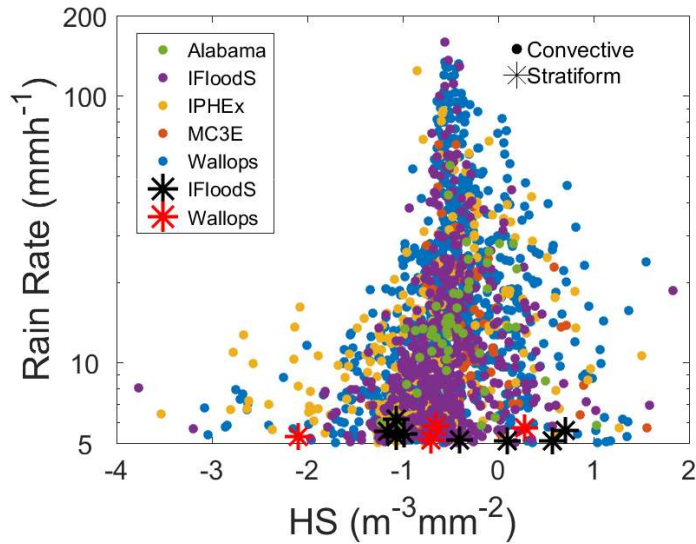


218 Figure 2. Distribution of drop diameter corresponding to  $HS > 0$  when the identification algorithm  
 219 (D'Adderio et al., 2015) is applied to 0.6-5 mm range.

Several arguments makes the effects of sorting unlikely in shaping the DSD: 1) the 2DVD sampling volume is rather small (around  $11 \text{ m}^3$  for largest drops), and thus making influences of size sorting in rain volumes unlikely, as it is more common in radar data (Dawson et al., 2015); 2) generally size sorting DSD presents a marked peak for large drops (2 mm of diameter or more), and with few drops at small size (Kumjian and Ryzhkov, 2012). Among the 352 DSD only 18 show a signal that can be due to size sorting contamination, with the peak at larger size (above 1.3 mm) higher than the peak at smaller drop size, while we never observed DSD with single peak at diameters larger than 2 mm. Finally, the possible contamination from DSD shaped by the coexistence of melted ice flakes and supercooled drops (or other anomalous distribution of frozen hydrometeors aloft) is unlikely, given the fact that the freezing level during the considered events is always higher than 2500 m a.s.l..

#### 4. Results

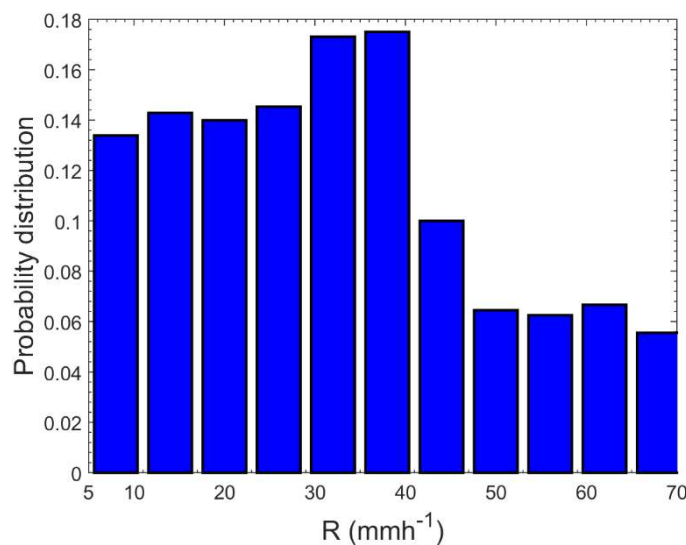
A first analysis was devoted to assess the occurrence of EDSD in convective and stratiform events: Figure 3 shows each sample according to its rain rate and HS value. EDSD occurrence in stratiform events is very rare and only three events in IFloodS and Wallops datasets (see Table 2) reported only three samples with EDSD (i.e.  $HS > 0$ ). The rain rate of the EDSD (i.e.  $HS > 0$ ) ranges mainly between 5 and  $70 \text{ mm h}^{-1}$ , while at higher rain rates, even exceeding  $100 \text{ mm h}^{-1}$ , the HS values is centered around  $-0.5 \text{ mm}^{-3}\text{m}^{-2}$ . In general, higher rain rates have lower HS values even if positive, while lower rain rates can reach HS values larger than one, indicating a marked two-peak DSD.



241 Figure 3. Distribution of the samples belonging to the selected events according to their rain rate  
 242 and HS. Dots indicate convective samples, while stars indicate stratiform samples.

243 The dependence of EDSO occurrence on the rain rate is presented by considering the fraction of  
 244 EDSO samples as function of the rain rate sampled over  $6 \text{ mm h}^{-1}$  wide intervals (Figure 4). The  
 245 fractional occurrence of EDSO slightly increases with the rainfall rate to reach a maximum above  
 246  $17\%$  around  $40 \text{ mm h}^{-1}$ , while the probability to have EDSO decreases below  $10\%$  at higher rain rates.

247



248 Figure 4. Fractional occurrence of samples with EDSO ( $HS > 0$ ) as function of the corresponding rain  
 249 rate.

The onset of EDSD seems to be weakly related to rainfall intensity above the threshold used. To assess if the EDSD is sensitive to the change of the rainfall intensity, the percent rain rate difference between two consecutive samples is calculated and, for each value, the percentage of samples with EDSD is reported at 20% intervals (Figure 5). Results indicate that a sudden increase of precipitation rate (especially between 100 and 200%) is favorable to the occurrence of EDSD. The samples where the rainfall rate increases between 120 and 200% have the probability higher than 30% to have EDSD, with a peak of 45% for a relative increase of rain rate of 150%. A sudden decrease of rainfall rate between two consecutive samples, shows a very low occurrence (about 2%) of EDSD, as well very large positive rain rate variation (above 220%) does not present any EDSD.

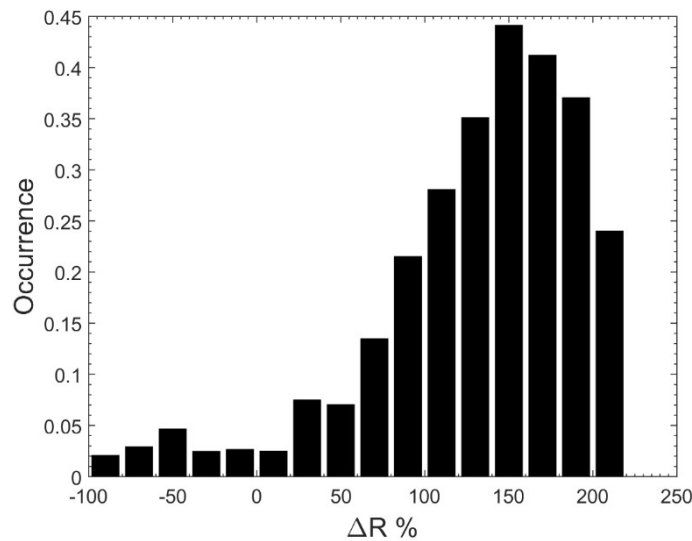
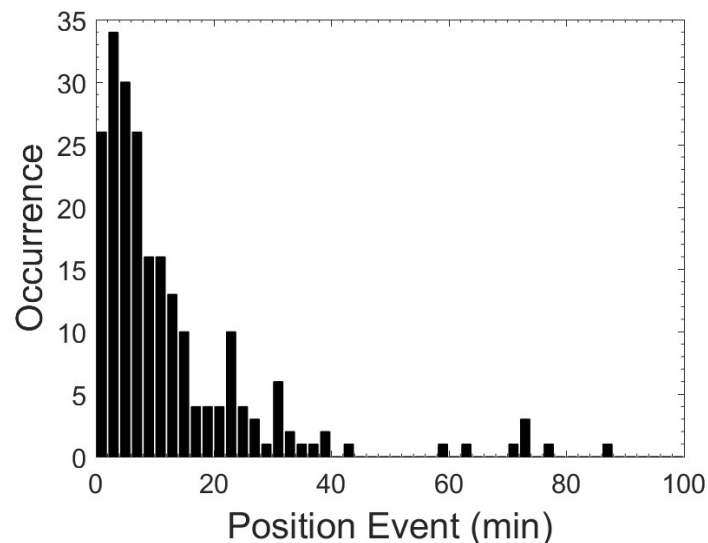


Figure 5. Fractional occurrence of samples with  $HS > 0$ , as function of the relative rain rate difference between each sample and the previous one.



265 A further analysis has been devoted to understand how the DSD evolves in time to reach the  
 266 equilibrium stage. The delay (in minutes) between the first rain detection for each event and the  
 267 appearance of the EDSD is computed for all the dataset (Figure 6). Each bar is two-minutes width  
 268 and it is centered in the middle value of the class (i.e. the first bar is centered at minute one and  
 269 indicated the detection of EDSD at first or second minute of the considered event).

270 The distribution is clearly peaked for time delays between 2 and 8 minutes after the precipitation  
 271 is first detected: for the 80% of the EDSD observation, it takes place within 20 minutes from the  
 272 start of the event observation, and in the 10% of the cases, the EDSD coincides with the first  
 273 observation of the event. There are also very few events for which the EDSD takes place after a long  
 274 time (between 60 and 90 minutes). EDSD was observed only once in an event in most of the  
 275 observations (75%), while two consecutive EDSD samples were present only in the 6% of the time.  
 276 Longer period with EDSD continuously detected are even rarer: 10 and 2 times (around 4 and 1% of  
 277 the EDSD samples) for 3 and 4 consecutive EDSD, respectively. Moreover, in the 15% of the cases  
 278 EDSD appears two or more times (not consecutively) in different stages of the same event.



279 Figure 6. Number of samples with  $HS > 0$  as function of the time difference with respect to the first  
 280 observation of the event (i.e.  $RR > 1 \text{ mm h}^{-1}$ ).

281

282 With our observing system (fixed and point-like measurements), however, we are not able to follow  
283 separately the spatial and time evolution of the same cloud column, and thus we cannot  
284 unambiguously assess the time needed to a given cloud column to reach the EDSD. This limitation  
285 prevents a deeper analysis of the results, and we discussed EDSD properties not affected by the  
286 inadequacy of the experimental settings. A field measurement designed for this purpose, however,  
287 would require a very high density disdrometers network with a focused spatial distribution and a  
288 dedicated radar with a high temporal resolution (given the fast response of the transient EDSD) to  
289 follow the evolution of the precipitation pattern.

290

## 291 5. Case studies

292 Times series of rain rate and HS are presented for three cases: two illustrate how the EDSD is  
293 reached in convective cases, and one will describe a stratiform case where the EDSD is not reached  
294 despite its long duration.

### 295 5.1 Convective events

296 The convective events selected show at least one EDSD spectrum during their lifetime. The time  
297 evolution of HS can be explained according to the time of observation of the EDSD occurrence with  
298 respect to the rain rate peak and the start of the observation. The analysis leads to the division of  
299 the selected events in two main groups.

300 For the events belonging to the first group, rainrate is already high at the first observation, and the  
301 HS is positive in one of the first samples: in more than 10% of the cases (Figure 6), the first sample  
302 observed in an event has a relatively large positive HS value, indicating that the EDSD is found in  
303 proximity of the edge of the rain pattern at the beginning of the rain event observation. We interpret

304 this behavior as follows: the rain system overpasses the instrument when the rain column already  
305 reached a mature stage. Often rain rate keeps increasing with time while HS drops below zero,  
306 indicating that the EDSD is lost due to the passage of the most intense part of the weather system  
307 over the instrument.

308 The second group of events is characterized by light/moderate rain rate and negative HS value at  
309 the beginning of the observation, rain rate increases more slowly with time, and reaches maximum  
310 values within 15-25 minutes after the first observation. HS increases in parallel with rain rate,  
311 reaching a positive value in correspondence with the maximum rain rate. We observe, in this case,  
312 the transition between negative and positive HS values, related to the increase of rain rate.

313 We present two case studies to illustrate the first and second group.

314 The event occurred on October 20, 2013 during the IFloodS field campaign is an example of well-  
315 defined convective event, belonging to the first group, where rain rates reached  $160 \text{ mm h}^{-1}$  (Figure  
316 7a). Measured rain rate increased from 4 to  $44 \text{ mm h}^{-1}$  in two minutes, and the first positive HS value  
317 was found by the algorithm at minute 204. The HS then dropped down below zero indicating that  
318 the EDSD signal was lost while rain rate further increased, and HS oscillates around  $-0.5 \text{ m}^{-3}\text{mm}^{-2}$   
319 after the peak rain rate ( $R = 159 \text{ mm h}^{-1}$ ) at minute 210. A close inspection of the DSD of minute 204  
320 and minute 210 (Figure 7b), shows an EDSD with a marked depletion of drops around 2 mm, that  
321 evolves to a DSD with much more drops until 4.5 mm and a well-defined slope. However, a weak  
322 change of concavity is present between 1 and 3 mm, indicating that other processes (Radhakrishna  
323 and Rao 2009), occurring during such intense episodes, affect the equilibrium between breakup and  
324 coalescence, and prevent the maintenance of the EDSD.

325

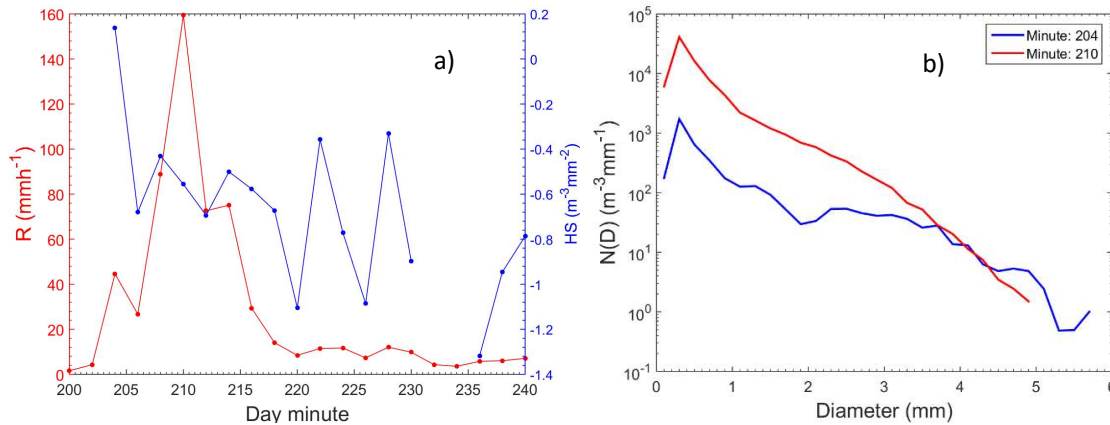


Figure 7. a) Time series of rain rate (red dot-line) and HS (blue dot-line) values, and b) DSDs of two samples of a rain event occurred on May 20, 2013 during IFloodS field campaign.

A second convective case, occurred on May 15, 2014 during the IPHEX field campaign, is reported to represent the second groups of events. In this case, HS reached its positive value at the peak of rain rate. The HS constantly increases from the beginning of the observation (except for one sample where a marked decrease of HS is related to a marked decrease of rain rate), up to reach a positive value. The precipitation peak reaches lower value with respect to the previous case, and this is a general difference between the two groups: the average peak intensity is  $60.6 \text{ mmh}^{-1}$  and  $36.3 \text{ mmh}^{-1}$  for the first and the second group, respectively. On the other hand, the mean rain rate of the EDSD samples does not show any difference for the two groups, with  $14.8$  and  $13.8 \text{ mmh}^{-1}$  for the first and second group, respectively. The higher rain rates do not seem support the developing and maintaining of EDSD. Furthermore, this case also confirms the transient nature of the EDSD, with its extremely short duration (only one sample).

The analysis of the DSD (Figure 8b) shows a clear transition from a well-defined Gamma distribution shape at minute 380 (green line) and at minute 382 (red line), both with  $\mu$  parameter around 4.8, to a bi-modal shape indicating the EDSD occurrence. Minute 384 (blue line) evidences the breakup effects with a concavity change already present leading to EDSD at minute 386 (black line).

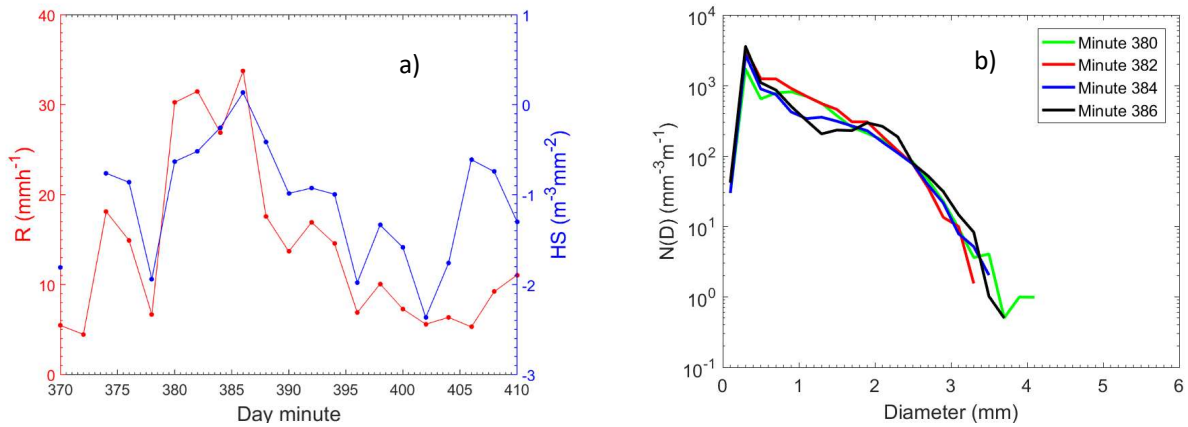


Figure 8. a) The same of Figure 6a, but for the event occurred on May 15, 2014 during IPHEX field campaign; b) DSDs preceding the equilibrium stage and EDSD.

## 5.2 Stratiform episode

The time evolution of rain rate and HS is shown for a stratiform case, occurred on December 29, 2013 at Wallops Island, Virginia, not classified as event since HS never reaches positive values (Figure 9). This case was observed for more than one hour and the rain rate was between 5 and 10  $\text{mm h}^{-1}$ . The HS parameter at the beginning of the observation had high negative value, indicating a very steep DSD, with a relatively large amount of small drops and no drops with diameter larger than 2 mm. The HS increases rapidly, indicating the formation of larger drops, as effect of coalescence, and then keeps increasing slowly with time, reaching the highest value after 60 minutes of nearly constant rain intensity, still lower than zero (Figure 9a). This shows that along the event the DSD modifies, reducing the slope of the curve between 1.0 and 2.6 mm. Comparing our results with Prat and Barros (2009) numerical simulations, this case demonstrates that time necessary to reach the EDSD during a stratiform event could be much longer with respect to a convective event.

The DSD of the considered event does not present any particular characteristic (Figure 9b). The measured drop diameters are generally lower than 3.5 mm, well below the breakup size (Porcù et al, 2013), therefore no bi-modal shape can be identified within this event.

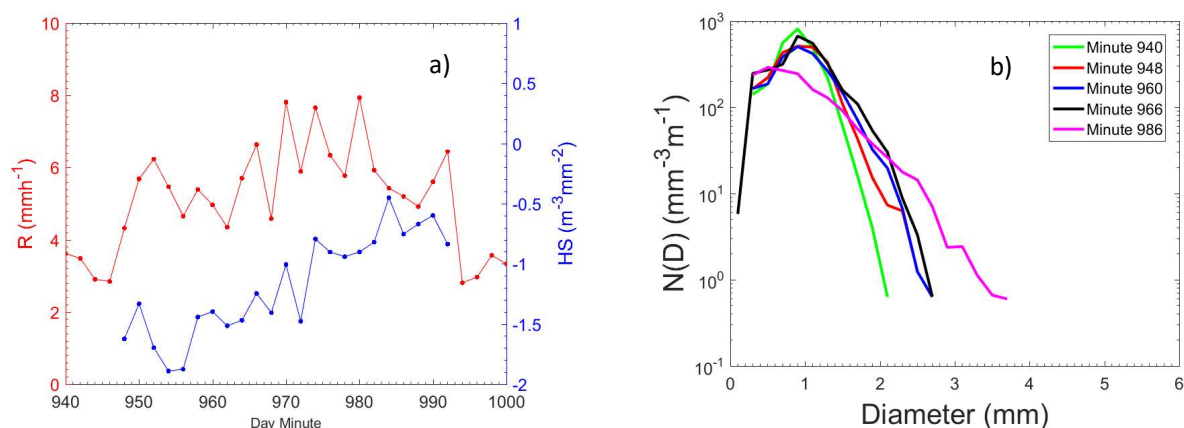


Figure 9. a) The same of Figure 6a, but for December 29, 2013 at Wallops Island, Virginia; b) sampling of DSDs for the whole period of observation.

## Conclusions

High density, high quality disdrometric datasets have been analyzed to investigate the DSD dynamics in natural rain. A specific algorithm developed to identify bi-modal DSD is applied to more than 6,000 minutes of liquid precipitation 2DVD measurements collected in different seasons and locations. We propose a number of arguments to assess that these bi-modal DSD are EDSD, allowing the analysis of their temporal characteristics.

Our results demonstrate that EDSD is reached almost exclusively in convective rain (128 convective events and 3 stratiform events), and confirm that the onset of EDSD is a rare event in natural rain (Prat and Barros, 2012) occurring at most around 7% of the times (D'Adderio et al., 2015).

We found that EDSD shows up few minutes after the start of the observation (about 66% in the first 10 minutes), indicating that EDSD is more likely to take place in the proximity of the external edge of the rain area. Since most of the considered events have a total duration of around 20-30 minutes, thus, we can extrapolate that the onset of the EDSD is expected to take place 10-15 minutes after the beginning of the precipitation, confirming the time scales suggested by numerical modeling.

A second relevant feature is the short lifetime of the EDSD, observed in only one 2-minute sample in most of the cases (about 75% of the cases). EDSD, moreover, is often detected in cases of relatively rapid precipitation rate increase. The probability to have an EDSD exceeds 25% for those samples presenting a rain rate increase of more than 100% with respect to the previous sample, with a relative maximum higher than 45% of EDSD occurrence when the fractional increase of rain rate is around 150%. In the case of the maximum rain rate observed is very high (above 50 mm h<sup>-1</sup>) the EDSD signal is lost, due to a number of mechanisms of higher order of complexity with respect to the coalescence-breakup balance (Radhakrishna and Rao 2009). If the rainfall rate remains limited below 50 mm h<sup>-1</sup>, is more frequent to find the EDSD in correspondence to the maximum rain rate.

For a group of events the instrument does not observe the precipitation onset: at a certain stage of the precipitation column life, the system reaches the instrument (we deducted this since the first sample presented high rain rate values) and the measurement starts from the external part of the rain column, where EDSD is detected. For a second group of events, the instrument observes the early stages of precipitation development until a maximum rain rate is reached: HS grows with rain intensity (starting from very low values) and maximum rainrate and EDSD are observed at the same time. In case of stratiform episodes, the DSD changes in time, increasing the drop size, but reaches equilibrium in only three cases.

The observation of the time evolution of DSD in natural rain is a difficult task, since it would need Lagrangian measurements of the cloud column. With our Eulerian approach, however, we assess some basic properties of the onset of the EDSD, compatible with numerical modeling and laboratory results. The results and related comments we reported in this work would be confirmed by an ad hoc experimental campaign, which seems, however, difficult to design and carry on.

#### Acknowledgements

This study was partially funded by the “The Foundation BLANCEFLOR Boncompagni Ludovisi, née Bildt”. Thanks to Patrick N. Gatlin of NASA Marshall Space Flight Center and Matthew Wingo of the University of Alabama at Huntsville for maintenance of 2DVD during NASA Global Precipitation Measurement (GPM) mission ground validation field campaigns led by Walter Petersen of NASA Wallops Flight Facility.

#### References

Barros, A. P., Pratt O. P., and Testik F. Y., 2010: Size distribution of raindrops. *Nat. Phys.*, 6, 232.

Bringi V.N., Chandrasekar V., Hubbert J., Gorgucci E., Randeu W. L., and Schoenhuber M., 2003: Raindrop Size Distribution in Different Climatic Regimes from Disdrometer and Dual-Polarized Radar Analysis. *J. Atmos. Sci.*, 60, 354–365.

Brown, P. S., Jr., 1988: The effects of filament, sheet, and disk breakup upon the drop spectrum. *J. Atmos. Sci.*, 45, 712–718, doi: 10.1175/1520-0469(1988)045<0712:TEOFSA>2.0.CO;2.



424 Caracciolo, C., Prodi, F., Battaglia, A., Porcù, F., 2006. Analysis of the moments and parameters of a  
425 gamma DSD to infer precipitation properties: a convective stratiform discrimination algorithm.  
426 Atmos. Res. 80 (2–3), 165–186.

427

428 Caracciolo, C., Napoli M., Porcù F., Prodi F., Dietrich S., Zanchi C. and Orlandini S., 2012: Raindrop  
429 size distribution and soil erosion. J. Irrig. Drain Eng., 138, 461-469.

430

431 Chen, J.-P. and Lamb D., 1994: Simulation of Cloud Microphysical and Chemical Processes Using a  
432 Multicomponent Framework. Part I: Description of the Microphysical Model. J. Atmos. Sci., 51,  
433 2613-2630, DOI: [http://dx.doi.org/10.1175/1520-0469\(1994\)051<2613:SOCMAC>2.0.CO;2](http://dx.doi.org/10.1175/1520-0469(1994)051<2613:SOCMAC>2.0.CO;2).

434

435 D’Adderio L.P., Porcù F. and Tokay A., 2015: Identification and analysis of collisional break-up in  
436 natural rain. J. Atmos. Sci., 72, 3404-3416, DOI: 10.1175/JAS-D-14-0304.1.

437

438 Dawson, D.T. II, Mansell, E.R. and Kumjian, M.R., 2015: Does wind shear cause hydrometeor size  
439 sorting, J. Atmos. Sci., 72, 340-348

440

441 Feingold G., Tzivion (Tzitzvashvili) S. and Leviv Z., 1988: Evolution of Raindrop Spectra. Part I:  
442 Solution to the Stochastic Collection/Breakup Equation Using the Method of Moments. J. Atmos.  
443 Sci., 45, 3387-3399, DOI: [http://dx.doi.org/10.1175/1520-0469\(1988\)045<3387:EORSPI>2.0.CO;2](http://dx.doi.org/10.1175/1520-0469(1988)045<3387:EORSPI>2.0.CO;2)

444

445 Ioannidou M.P., Kalogiros J.A., Stavrakis A.K., 2016: Comparison of the TRMM Precipitation Radar  
446 rainfall estimation with ground-based disdrometer and radar measurements in South Greece.

447 Atmos. Res., 181, 172-185, DOI: <http://dx.doi.org/10.1016/j.atmosres.2016.06.023>

448

449 Kumjian M.R. and Ryzhkov A.V., 2012: The Impact of Size Sorting on the Polarimetric Radar  
450 Variables. J. Atmos. Sci., 69, 2042-2060. DOI: 10.1175/JAS-D-11-0125.1

451

452 Low, T. B., and List R., 1982a: Collision, coalescence and breakup of raindrops. Part I: Experimentally  
453 established coalescence efficiencies and fragment size distributions in breakup. J. Atmos. Sci., 39,  
454 1591–1606, doi:10.1175/1520-0469(1982)039,1591:CCABOR.2.0.CO;2.

455

456 Low, T. B., and List R., 1982b: Collision, coalescence and breakup of raindrops. Part II:  
457 Parameterizations of fragment size distributions. J. Atmos. Sci., 39, 1607–1618, doi:10.1175/ 1520-  
458 0469(1982)039,1607:CCABOR.2.0.CO;2.

459

460 McFarquhar G. M., 2004: A new representation of collision-induced breakup of raindrops and its  
461 implications for the shapes of raindrop size distributions. J. Atmos. Sci., 61, 777–794.

462

463 McTaggart-Cowan, J.D. and List R., 1975: Collision and breakup of water drops at terminal velocity.  
464 J. Atmos. Sci., 32, 1401–1411.

465

466 Porcù, F., D’Adderio L. P., Prodi F. and Caracciolo C., 2013, Effects of altitude on maximum raindrop  
467 size and fall velocity as limited by collisional breakup, J. Atmos. Sci., 70, 1129-1134.

468

469 Porcù, F., D’Adderio L. P., Prodi F. and Caracciolo C., 2014, Rain drop size distribution over the  
470 Tibetan Plateau, Atmos. Res., 150, 21-30.

471

472 Prat, O. P. and Barros A. P., 2007: A Robust Numerical Solution of the Stochastic Collection–Breakup  
473 Equation for Warm Rain. *J. App. Meteor. Climatol.* 46, 1480-1497.

474

475 Prat, O. P. and Barros A. P., 2009: Exploring the transient behavior of Z-R relationships-Implications  
476 for Radar Rainfall Estimation. *J. Applied Meteor. and Clim.*, 48, 2127-2143.

477

478 Prat, O. P., Barros A. P. and Testik F., 2012: On the influence of raindrop collision outcomes on  
479 equilibrium size distributions. *J. Atmos. Sci.*, 69, 1534–1546, doi:10.1175/JAS-D-11-0192.1.

480

481 Radhakrishna, B., and Rao T. N., 2009: Statistical characteristics of multipeak raindrop size  
482 distributions at the surface and aloft in different rain regimes. *Mon. Wea. Rev.*, 137, 3501–3518,  
483 doi:10.1175/2009MWR2967.1.

484

485 Schlottke, J., Straub W., Beheng K., Goma H., and Weigand B., 2010: Numerical investigation of  
486 collision-induced breakup of raindrops. Part I: Methodology and dependencies on collision energy  
487 and eccentricity. *J. Atmos. Sci.*, 67, 557–575, doi:10.1175/2009JAS3174.1.

488

489 Schönhuber, M., Lammer G., and Randeu W. L., 2007: One decade of imaging precipitation  
490 measurement by 2Dvideo-disdrometer. *Adv. Geosci.*, 10, 85–90, doi:10.5194/adgeo-10-85-2007.

491

492 Steiner, M. and Waldvogel A., 1987: Peaks in Raindrop Size Distributions. *J. Atmos. Sci.*, 44, 3127-  
493 3133, DOI: [http://dx.doi.org/10.1175/1520-0469\(1987\)044<3127:PIRSD>2.0.CO;2](http://dx.doi.org/10.1175/1520-0469(1987)044<3127:PIRSD>2.0.CO;2).

494

495 Tao, W.-K., Lang S., Zeng X., Li X., Matsui T., Mohr K., Posselt D., Chern J., Peters-Lidard C., Norris  
 496 P.M., Kang I.-S., Choi E., Hou A., Lau K.-M. and Yang Y.-M., 2014: The Goddard Cumulus Ensemble  
 497 model (GCE): Improvements and applications for studying precipitation processes. *Atmos. Res.*, 143,  
 498 392–424

499 Thurai M., Gatlin P.N., Bringi V.N., 2016. Separating stratiform and convective rain types based on  
 500 the drop size distribution characteristics using 2D video disdrometer data. *Atmos.Res.*, 169, 416-  
 501 423. DOI: <http://dx.doi.org/10.1016/j.atmosres.2015.04.011>  
 502

503 Tokay, A., W. A. Petersen, P. Gatlin, and M. Wing, 2013: Comparison of raindrop size distribution  
 504 measurements by collocated disdrometers. *J. Atmos. Oceanic Technol.*, 30, 1672-1690.  
 505

506 Tokay, A., D’Adderio L.P., Wolff D. B. and Petersen W. A., 2016: A Field Study of Pixel-Scale Variability  
 507 of Raindrop Size Distribution in the Mid-Atlantic Region. *J. Hydrometeo.*, 17, 1855-1868, DOI:  
 508 <http://dx.doi.org/10.1175/JHM-D-15-0159.1>.  
 509

510 Valdez, M. P., and Young K. C., 1985: Number fluxes in equilibrium raindrop populations: A Markov  
 511 chain analysis. *J. Atmos. Sci.*, 42, 1024–1036, doi:10.1175/1520-  
 512 0469(1985)042<1024:NFIERP>2.0.CO;2.  
 513

514 Willis, P. T., and Tattelman P., 1989: Drop-size distributions associated with intense rainfall. *J. Appl.*  
 515 *Meteor.*, 28, 3–15, doi:10.1175/1520-0450(1989)028<0003:DSDAWI>2.0.CO;2.  
 516

517 Zawadzki, I., and De Agostinho Antonio M., 1988: Equilibrium raindrop size distributions in tropical  
 518 rain. *J. Atmos. Sci.*, 45, 3452–3459, doi:10.1175/1520-0469(1988)045<3452:ERSDIT>2.0.CO;2.



520 Captions

521 Figure 1. PDF (blue lines) and CDF (red lines) for convective (solid lines) and stratiform (dashed lines)  
522 samples.

523

524 Figure 2. Distribution of drop diameter corresponding to  $HS > 0$  when the identification algorithm  
525 (D'Adderio et al., 2015) is applied to 0.6-5 mm range.

526

527 Figure 3. Distribution of the samples belonging to the selected events according to their rain rate  
528 and HS. Dots indicate convective samples, while stars indicate stratiform samples.

529

530 Figure 4. Fractional occurrence of samples with ESD ( $HS > 0$ ) as function of the corresponding rain  
531 rate.

532

533 Figure 5. Fractional occurrence of samples with  $HS > 0$ , as function of the relative rain rate difference  
534 between each sample and the previous one.

535

536 Figure 6. Number of samples with  $HS > 0$  as function of the time difference with respect to the first  
537 observation of the event (i.e.  $RR > 1 \text{ mm h}^{-1}$ ).

538

539 Figure 7. a) Time series of rain rate (red dot-line) and HS (blue dot-line) values, and b) DSDs of two  
540 samples of a rain event occurred on May 20, 2013 during IFloodS field campaign.

541

542 Figure 8. a) The same of Figure 6a, but for the event occurred on May 15, 2014 during IPHEX field  
543 campaign; b) DSDs preceding the equilibrium stage and EDSD.

544

545 Figure 9 a) The same of Figure 6a, but for December 29, 2013 at Wallops Island, Virginia; b) sampling  
546 of DSDs for the whole period of observation.